Doxycycline has Distinct Apicoplast-Specific Mechanisms of Antimalarial Activity

Megan Okada[a], Ping Guo[a], Shai-anne Nalder[a], and Paul A. Sigala[a,1]

[a]Department of Biochemistry, University of Utah School of Medicine, Salt Lake City, UT 84112

[1]To whom correspondence may be addressed: p.sigala@biochem.utah.edu

ORCID ID:
(M.O.) 0000-0003-4398-9819
(P.G.) 0000-0003-3023-779X
(S.N.) 0000-0002-6892-9321
(P.A.S.) 0000-0002-3464-3042

Author contributions: P.A.S. designed research; P.G., S.N., M.O., and P.A.S. performed research and analyzed data; P.A.S. wrote the paper.

The authors declare no competing interests.

Abstract: Doxycycline (DOX) is a key antimalarial drug thought to kill *Plasmodium* parasites by blocking protein translation in the essential apicoplast organelle. Clinical use is primarily limited to prophylaxis due to delayed second-cycle parasite death at 1-3 μM serum concentrations. DOX concentrations >5 μM kill parasites with first-cycle activity but have been ascribed to off-target mechanisms outside the apicoplast. We report that 10 μM DOX blocks apicoplast biogenesis in the first cycle and is rescued by isopentenyl pyrophosphate, an essential apicoplast product, confirming an apicoplast-specific mechanism. Exogenous iron rescues parasites and apicoplast biogenesis from first- but not second-cycle effects of 10 μM DOX, revealing that first-cycle activity involves a metal-dependent mechanism distinct from the delayed-death mechanism. These results critically expand the paradigm for understanding the fundamental antiparasitic mechanisms of DOX and suggest repurposing DOX as a faster-acting antimalarial at higher dosing whose multiple mechanisms would be expected to limit parasite resistance.

68 **INTRODUCTION**

69 Malaria remains a serious global health problem, with hundreds of thousands of annual deaths due
70 to *Plasmodium falciparum* parasites. The absence of a potent, long-lasting vaccine and parasite
71 tolerance to frontline artemisinin combination therapies continue to challenge malaria elimination
72 efforts. Furthermore, there are strong concerns that the current COVID-19 pandemic will disrupt
73 malaria prevention and treatment efforts in Africa and cause a surge in malaria deaths that unravels
74 decades of progress (1). Deeper understanding of basic parasite biology and the mechanisms of
75 current drugs will guide their optimal use for malaria prevention and treatment and facilitate
76 development of novel therapies to combat parasite drug resistance.

77 Tetracycline antibiotics like DOX are thought to kill eukaryotic *P. falciparum* parasites by
78 inhibiting prokaryotic-like 70S ribosomal translation inside the essential apicoplast organelle
79 (Figure 1) (2). Although stable *P. falciparum* resistance to DOX has not been reported, clinical use
80 is largely limited to prophylaxis due to delayed activity against intraerythrocytic infection (3, 4).
81 Parasites treated with 1-3 μM DOX, the drug concentration sustained in human serum with current
82 100-200 mg dosage (5), continue to grow for 72-96 hours and only die after the second 48-hour
83 intraerythrocytic growth cycle when they fail to expand into a third cycle (2). Slow antiparasitic
84 activity is believed to be a fundamental limitation of DOX and other antibiotics that block
85 apicoplast-maintenance pathways (4, 6). First-cycle anti-*Plasmodium* activity has been reported
86 for DOX and azithromycin concentrations >3 μM, but such activities have been ascribed to targets
87 outside the apicoplast (2, 7, 8). A more incisive understanding of the mechanisms and parameters
88 that govern first versus second-cycle DOX activity can inform and improve clinical use of this
89 valuable antibiotic for antimalarial treatment. We therefore set out to test and unravel the
90 mechanisms and apicoplast specificity of first-cycle DOX activity.

91 **RESULTS AND DISCUSSION**

92 **First-cycle activity by 10 μM DOX has an apicoplast-specific mechanism.** Prior studies have
93 shown that 200 μM isopentenyl pyrophosphate (IPP), an essential apicoplast product, rescues
94 parasites from the delayed-death activity of 1-3 μM DOX, confirming an apicoplast-specific target
95 (7). To provide a baseline for comparison, we first used continuous-growth and 48-hour growth-
96 inhibition assays to confirm that IPP rescued parasites from 1 μM DOX (Figure 2A) and that DOX
97 concentrations >5 μM killed parasites with first-cycle activity (Figure 2A – C and Figure 2- figure
98 supplement 1) as previously reported (2). To test the apicoplast specificity of first-cycle DOX
99 activity, we next asked whether 200 μM IPP could rescue parasites from DOX concentrations >5
100 μM. We observed that IPP shifted the 48-hour EC_{50} value of DOX from 5 ± 1 to 12 ± 2 μM
101 (average ± SD of 5 independent assays, P = 0.001 by unpaired t-test) (Figure 2C and Figure 2-
102 figure supplement 1), suggesting that first-cycle growth defects from 5-10 μM DOX reflect an
103 apicoplast-specific mechanism but that DOX concentrations >10 μM cause off-target defects
104 outside this organelle. We further tested this conclusion using continuous growth assays performed
105 at constant DOX concentrations. We observed that IPP fully or nearly fully rescued parasites from
106 first-cycle growth inhibition by 10 μM but not 20 or 40 μM Dox (Figure 2A & 2D and Figure 2-
107 figure supplement 1). On the basis of IPP rescue, we conclude that 10 μM DOX kills *P. falciparum*
108 with first-cycle activity by an apicoplast-specific mechanism.

109

110 **10 μM DOX blocks apicoplast biogenesis in the first cycle:** Inhibition of apicoplast biogenesis
111 in the second intraerythrocytic cycle is a hallmark of 1-3 μM DOX-treated *P. falciparum*, resulting
112 in unviable parasite progeny that fail to inherit the organelle (2). IPP rescues parasite viability after
113 the second cycle without rescuing apicoplast inheritance, such that third-cycle daughter parasites

114 lack the organelle and accumulate apicoplast-targeted proteins in cytoplasmic vesicles (7). We
115 treated synchronized ring-stage D10 (9) or NF54 (10) parasites expressing the acyl carrier protein
116 leader sequence fused to GFP (ACP_L-GFP) with 10 μM DOX and assessed apicoplast morphology
117 30-36 hours later in first-cycle schizonts. In contrast to the second-cycle effects of 1-3 μM DOX,
118 the apicoplast in 10 μM DOX-treated parasites failed to elongate in the first cycle. Rescue by 200
119 μM IPP produced second-cycle parasite progeny with a dispersed GFP signal indicative of
120 apicoplast loss (Figure 2E and Figure 2- figure supplement 2). We conclude that 10 μM DOX
121 blocks apicoplast biogenesis in the first cycle.
122
123 **First- and second-cycle effects of DOX on the apicoplast are due to distinct mechanisms.**
124 What is the molecular mechanism of faster apicoplast-specific activity by 10 μM DOX? We first
125 considered the model that both 1 and 10 μM DOX inhibit apicoplast translation but that 10 μM
126 DOX kills parasites faster due to more stringent translation inhibition at higher drug
127 concentrations. This model predicts that treating parasites simultaneously with multiple distinct
128 apicoplast-translation inhibitors, each added at a delayed death-inducing concentration, will
129 produce additive, accelerated activity that kills parasites in the first cycle. To test this model, we
130 treated synchronized D10 parasites with combinatorial doses of 2 μM DOX, 2 μM clindamycin,
131 and 500 nM azithromycin and monitored growth over 3 intraerythrocytic cycles. Treatment with
132 each antibiotic alone produced major growth defects at the end of the second cycle, as expected
133 for delayed-death activity at these concentrations (6). Two- and three-way drug combinations
134 caused growth defects that were indistinguishable from individual treatments and provided no
135 evidence for additive, first-cycle activity (Figure 3A and Figure 3- figure supplement 1). These

136 results contradict a simple model that 1 and 10 μM DOX act via a common translation-blocking
137 mechanism and suggest that the first-cycle activity of 10 μM DOX is due to a distinct mechanism.
138
139 **Exogenous iron rescues parasites from first- but not second-cycle effects of 10 μM DOX.**
140 Tetracycline antibiotics like DOX tightly chelate a wide variety of di- and trivalent metal ions via
141 their siderophore-like arrangement of exocyclic hydroxyl and carbonyl groups (Figure 1), with a
142 reported affinity series of Fe^{3+}>Fe^{2+}>Zn^{2+}>Mg^{2+}>Ca^{2+} (11, 12). Indeed, tetracycline interactions
143 with Ca^{2+} and Mg^{2+} ions mediate cellular uptake and binding to biomolecular targets such as the
144 tetracycline repressor and 16S rRNA (12, 13). We next considered a model that first-cycle effects
145 of 10 μM DOX reflect a metal-dependent mechanism distinct from ribosomal inhibition causing
146 second-cycle death. To test this model, we investigated whether exogenous metals rescued
147 parasites from 10 μM DOX. We failed to observe growth rescue by 10 μM $ZnCl_2$ (toxicity limit
148 (14)) or 500 μM $CaCl_2$ in continuous-growth (Figure 3B and Figure 3- figure supplement 1) or 48-
149 hour growth-inhibition assays (Figure 3C). In contrast, 500 μM $FeCl_3$ (and to a lesser extent 500
150 μM $MgCl_2$) fully or nearly fully rescued parasites from first-cycle growth inhibition by 10 μM
151 DOX (Figure 3C & 3D), although partial rescue was observed at $FeCl_3$ concentrations as low as
152 50 μM (Figure 3- figure supplement 1). However, parasites treated with 10 μM DOX and 500 μM
153 $FeCl_3$ still succumbed to second-cycle, delayed death (Figure 3D and Figure 3- figure supplement
154 1), as expected for distinct mechanisms of first- and second-cycle DOX activity.
155 We also observed that 500 μM $FeCl_3$ but not $CaCl_2$ rescued first-cycle apicoplast-
156 branching in 10 μM DOX (Figure 3E and Figure 3- figure supplement 2). These observations
157 contrast with IPP, which rescued parasite viability in 10 μM DOX but did not restore apicoplast
158 branching (Figure 2E). We further noted that $FeCl_3$ selectively rescued parasites from the

159 apicoplast-specific, first-cycle growth effects of 10 μM DOX but did not rescue parasites from the
160 second-cycle effects of 1 μM DOX (Figures 3F) or the off-target effects of 20-40 μM DOX (Figure
161 3G and Figure 3- figure supplement 1). We conclude that 10 μM DOX kills parasites via a metal-
162 dependent, first-cycle mechanism that blocks apicoplast biogenesis and is distinct from the second-
163 cycle, delayed-death mechanism of 1 μM DOX.
164
165 **Metal-dependent mechanisms of first-cycle activity by 10 μM DOX.** What is the metal-
166 dependent mechanism of 10 μM DOX, and why is there preferential rescue by $FeCl_3$?
167 Tetracyclines bind iron more tightly than other metals, with an equilibrium association constant of
168 10^{10} M^{-1} for 1:1 chelation of Fe^{3+} versus 10^4 M^{-1} for Mg^{2+} (11). Although the 500 μM concentration
169 of exogenous $FeCl_3$ required for maximal rescue of parasite growth in 10 μM DOX is large relative
170 to the ~1 μM labile iron concentration estimated for the parasite cytoplasm (15), the intracellular
171 iron concentration achieved by exogenous addition of 500 μM $FeCl_3$ remains unclear. Indeed,
172 mechanisms of iron uptake and trafficking by blood-stage *P. falciparum* remain sparsely
173 understood (15, 16), especially uptake across the four membranes that surround the apicoplast.
174 We first considered whether exogenous $FeCl_3$ might selectively rescue 10 μM DOX
175 activity by blocking or reducing its uptake into the parasite apicoplast, since metal chelation has
176 been reported to influence the cellular uptake of tetracycline antibiotics in other organisms (12).
177 However, 500 μM $FeCl_3$ or $MgCl_2$ did not rescue second-cycle parasite death in continuous growth
178 assays with 10 μM (Figures 3D) or 1 μM DOX (Figure 3F). Furthermore, exogenous iron resulted
179 in only a small, 1.5-μM shift in EC_{50} value from 0.5 to 2 μM in a 96-hour growth inhibition assay,
180 in contrast to the 10.5-μM shift provided by IPP (Figure 3- figure supplement 1). These results
181 strongly suggest that DOX uptake into the apicoplast is not substantially perturbed by exogenous

182 iron. The inability of 500 μM $FeCl_3$ to rescue first-cycle activity by ≥20-μM DOX (Figure 3G)
183 further suggests that general uptake of DOX into parasites is not substantially affected by
184 exogenous iron.

185 We propose two distinct models to explain the metal-dependent effects of 10 μM DOX,
186 both of which could contribute to apicoplast-specific activity. First, DOX could directly bind and
187 sequester labile iron within the apicoplast, reducing its bioavailability for Fe-S cluster biogenesis
188 and other essential iron-dependent processes in this organelle. Indeed, prior work has shown that
189 apicoplast biogenesis requires Fe-S cluster synthesis apart from known essential roles in
190 isoprenoid biosynthesis (17). In this first model, rescue by exogenous $FeCl_3$ would be due to
191 restoration of iron bioavailability, while modest rescue by 500 μM $MgCl_2$ may reflect competitive
192 displacement of DOX-bound iron to restore iron bioavailability. RPMI growth medium already
193 contains ~400 μM Mg^{2+} prior to supplementation with an addition 500 μM $MgCl_2$, and thus Mg^{2+}
194 availability is unlikely to be directly limited by 10 μM DOX. Consistent with a general mechanism
195 that labile-iron chelation can block apicoplast biogenesis, we observed in preliminary studies that
196 the anti-*Plasmodium* growth inhibition caused by the highly-specific iron chelator, deferoxamine
197 (DFO) (16), could be partially rescued by IPP, fully rescued by exogenous $FeCl_3$, and involved a
198 first-cycle defect in apicoplast branching/division (Figure 3- figure supplement 3). Development
199 of targeted and incisive probes of labile iron within subcellular compartments remains an ongoing
200 challenge in biology (18), especially in the *Plasmodium* apicoplast where iron uptake,
201 concentration, and utilization remain sparsely understood. To evaluate the impact of DOX on iron
202 availability in the apicoplast, we are developing protein-based probes of lipoic acid and isoprenoid
203 biosynthesis, as these two apicoplast-dependent processes require Fe/S-cluster biosynthesis for
204 activity (17).

205 In a second model, DOX could bind to additional macromolecular targets within the
206 apicoplast (e.g., a metalloenzyme) via metal-dependent interactions that inhibit essential functions
207 required for organelle biogenesis. Exogenous 500 μM Fe^{3+} would then rescue parasites by
208 disrupting these inhibitory interactions via competitive binding to DOX. This second model would
209 be mechanistically akin to diketo acid inhibitors of HIV integrase like raltegravir that bind to active
210 site Mg^{2+} ions to inhibit integrase activity but are displaced by exogenous metals (19, 20). To test
211 this model, we are developing a DOX-affinity reagent to identify apicoplast targets that interact
212 with doxycycline and whose inhibition may contribute to first-cycle DOX activity.
213
214 **Conclusions and implications.** These results critically expand the paradigm for understanding the
215 fundamental mechanisms of DOX activity against *P. falciparum* malaria parasites. These
216 mechanisms include a delayed, second-cycle defect at 1-3 μM DOX that likely reflects inhibition
217 of 70S apicoplast ribosomes, a first-cycle iron-dependent defect within the apicoplast that uniquely
218 operates at 8-10 μM DOX, and a first-cycle iron-independent mechanism outside the apicoplast at
219 ≥20 μM DOX (Figure 1). Pharmacokinetic studies indicate that current 100-200 mg doses of DOX
220 achieve peak human serum concentrations of 6-8 μM over the first six hours which then decrease
221 to 1-2 μM over 24 hours (5). Although current DOX treatment regimens result in delayed parasite
222 clearance in vivo, both apicoplast-specific mechanisms of DOX likely operate over this
223 concentration range and contribute to parasite death (2). These multiple mechanisms of DOX,
224 together with limited antimalarial use of DOX in the field, may explain why parasites with stable
225 DOX resistance have not emerged (3, 4).
226 There has been a prevailing view in the literature that delayed-death activity is a
227 fundamental limitation of antibiotics like DOX that block apicoplast maintenance (21, 22). Our

228 results emphasize that DOX is not an intrinsically slow-acting antimalarial drug and support the
229 emerging paradigm (23-25) that inhibition of apicoplast biogenesis can defy the delayed-death
230 phenotype to kill parasites on a faster time-scale. The first-cycle, iron-dependent impacts of 10
231 μM DOX or 15 μM DFO on apicoplast biogenesis also suggest that this organelle may be
232 especially susceptible to therapeutic strategies that interfere with acquisition and utilization of iron,
233 perhaps due to limited uptake of exogenous iron and/or limited iron storage mechanisms in the
234 apicoplast.

235 Finally, this work suggests the possibility of repurposing DOX as a faster-acting
236 antiparasitic treatment at higher dosing, whose multiple mechanisms would be expected to limit
237 parasite resistance. Prior studies indicate that 500-600 mg doses in humans achieve sustained
238 serum DOX concentrations ≥5 μM for 24-48 hours with little or no increase in adverse effects (26,
239 27). DOX is currently contraindicated for long-term prophylaxis in pregnant women and young
240 children, two of the major at-risk populations for malaria, due to concerns about impacts on fetal
241 development and infant tooth discoloration, respectively, based on observed toxicities for other
242 tetracyclines (28). Recent studies suggest that these effects are not associated with short-term DOX
243 use (28, 29), but more work is needed to define the safety parameters that would govern short-term
244 use of DOX for treatment in these populations. Recent development of tetracycline derivatives
245 with improved activities may provide another option to deploy this important class of antibiotics
246 for antimalarial treatment (30).

247

248

249

250

251 **METHODS**

252 **Materials**: All reagents were cell-culture grade and/or of the highest purity commercially
253 available. The vendor and catalog number are given for individual compounds when first
254 mentioned.

255

256 **Parasite culture:** All experiments were performed using *Plasmodium falciparum* Dd2, ACP_L-
257 GFP D10 (9), or ACP_L-GFP NF54 (10) parasite strains. Parasite culturing was performed as
258 previously described (31) in Roswell Park Memorial Institute medium (RPMI-1640, Thermo
259 Fisher 23400021) supplemented with 2.5 g/L Albumax I Lipid-Rich BSA (Thermo Fisher
260 11020039), 15 mg/L hypoxanthine (Sigma H9636), 110 mg/L sodium pyruvate (Sigma P5280),
261 1.19 g/L HEPES (Sigma H4034), 2.52 g/L sodium bicarbonate (Sigma S5761), 2 g/L glucose
262 (Sigma G7021), and 10 mg/L gentamicin (Invitrogen Life Technologies 15750060). Cultures were
263 maintained at 2% hematocrit in human erythrocytes obtained from the University of Utah Hospital
264 blood bank, at 37 ˚C, and at 5% O_2, 5% CO_2, 90% N_2.

265

266 **Parasite Growth Assays:** Parasites were synchronized to the ring stage either by treatment with
267 5% D-sorbitol (Sigma S7900) or by first magnet-purifying schizonts and then incubating them
268 with uninfected erythrocytes for five hours followed by treatment with 5% D-sorbitol. Results
269 from growth assays using either of these synchronization methods were indistinguishable, and 5%
270 sorbitol was used for synchronization unless stated otherwise. For continuous growth assays,
271 parasite growth was monitored by diluting sorbitol-synchronized parasites to ~0.5% starting
272 parasitemia, adding additional treatments (antibiotics, IPP, and/or metal salts) at assay initiation,
273 and allowing culture expansion over several days with daily media changes. Growth assays with

274 doxycycline (Sigma D3447), clindamycin (Sigma C6427), and azithromycin (Sigma 75199) were
275 conducted at 0.2% DMSO at the indicated final drug concentration. Growth assays with $ZnCl_2$
276 (Sigma 208086), $CaCl_2$ (Sigma C4901), $MgCl_2$ (M8266), $FeCl_3$ (Sigma 236489), deferoxamine
277 (Sigma D9533), and/or IPP (NH_4^+ salt, Isoprenoids IPP001) were conducted at the indicated final
278 concentrations. Parasitemia was monitored daily by flow cytometry by diluting 10 µl of each
279 parasite culture well from 2-3 biological replicates into 200µl of 1.0 µg/ml acridine orange
280 (Invitrogen Life Technologies A3568) in phosphate buffered saline (PBS) and analysis on a BD
281 FACSCelesta system monitoring SSC-A, FSC-A, PE-A, FITC-A, and PerCP-Cy5-5-A channels.
282 For EC_{50} determinations via dose-response assay, synchronous ring-stage parasites were diluted
283 to 1% parasitemia and incubated with variable (serially two-fold diluted) DOX concentrations
284 ±200 µM IPP, ±50 µM mevalonate (Cayman 20348), ±500 µM $FeCl_3$, or ±500 µM $CaCl_2$ for 48-
285 120 hours without media changes. Parasitemia was determined by flow cytometry for 2-4
286 biological replicates for each untreated or drug-treated condition, normalized to the parasitemia in
287 the absence of drug, plotted as the average ±SD of biological replicates as a function of the log of
288 the drug concentration (in µM), and fit to a 4-parameter dose-response model using GraphPad
289 Prism 8.0. All growth assays were independently repeated 2-4 times on different weeks and in
290 different batches of blood. The 48-hour EC_{50} values determined from five independent assays for
291 DOX ±IPP were averaged and analyzed by unpaired t-test using GraphPad Prism 8.0.
292
293 **Fluorescence Microscopy:** For live-cell experiments, parasites samples were collected at 30-36
294 or 65 hours after synchronization with magnet purification plus sorbitol treatment (see above).
295 Imaging experiments were independently repeated twice. Parasite nuclei were visualized by
296 incubating samples with 1-2 µg/ml Hoechst 33342 (Thermo Scientific Pierce 62249) for 10-20

297 minutes at room temperature. The parasite apicoplast was visualized in D10 (9) or NF54
298 mevalonate-bypass (10) cells using the ACP_{leader}-GFP expressed by both lines. Images were taken
299 on DIC/brightfield, DAPI, and GFP channels using either a Zeiss Axio Imager or an EVOS M5000
300 imaging system. Fiji/ImageJ was used to process and analyze images. All image adjustments,
301 including contrast and brightness, were made on a linear scale. For indicated conditions, apicoplast
302 morphologies in 20-40 parasites were scored as elongated, focal, or dispersed; counted; and plotted
303 by histogram as the fractional population with the indicated morphology. Analysis of replicate
304 samples indicated standard deviations that were <10% for all samples in the percentage of
305 parasites displaying a given apicoplast morphology in a given condition. Unpaired t-test analysis
306 using GraphPad Prism was used to evaluate the significance of observed population differences.
307

308 **ACKNOWLEDGEMENTS.** We thank Jeremy Burrows, Dan Goldberg, Don Granger, Daria
309 Hazuda, Jerry Kaplan, Sean Prigge, Dennis Winge and members of the Sigala lab for helpful
310 discussions. P.A.S. holds a Career Award at the Scientific Interface from the Burroughs Wellcome
311 Fund and a Pew Biomedical Scholarship from the Pew Charitable Trusts. Microscopy and flow
312 cytometry were performed using core facilities at the University of Utah.
313

314 **References:**

315 1. Weiss DJ, *et al.* (2020) Indirect effects of the COVID-19 pandemic on malaria intervention
316 coverage, morbidity, and mortality in Africa: a geospatial modelling analysis. *Lancet Infect.*
317 *Dis.* http://dx.doi.org/10.1016/S1473-3099(20)30700-3.
318 2. Dahl EL, *et al.* (2006) Tetracyclines specifically target the apicoplast of the malaria parasite
319 Plasmodium falciparum. *Antimicrob. Agents Chemother.* 50(9):3124-3131.
320 http://dx.doi.org/10.1128/AAC.00394-06.
321 3. Conrad MD & Rosenthal PJ (2019) Antimalarial drug resistance in Africa: the calm before
322 the storm? *Lancet Infect. Dis.* 19(10):e338-e351. http://dx.doi.org/10.1016/S1473-
323 3099(19)30261-0.

4. Gaillard T, Madamet M, & Pradines B (2015) Tetracyclines in malaria. *Malar. J.* 14:445. http://dx.doi.org/10.1186/s12936-015-0980-0.
5. Newton PN, *et al.* (2005) Pharmacokinetics of oral doxycycline during combination treatment of severe falciparum malaria. *Antimicrob. Agents Chemother.* 49(4):1622-1625. http://dx.doi.org/10.1128/AAC.49.4.1622-1625.2005.
6. Dahl EL & Rosenthal PJ (2007) Multiple antibiotics exert delayed effects against the Plasmodium falciparum apicoplast. *Antimicrob. Agents Chemother.* 51(10):3485-3490. http://dx.doi.org/10.1128/AAC.00527-07.
7. Yeh E & DeRisi JL (2011) Chemical rescue of malaria parasites lacking an apicoplast defines organelle function in blood-stage Plasmodium falciparum. *PLoS Biol.* 9(8):e1001138. http://dx.doi.org/10.1371/journal.pbio.1001138.
8. Wilson DW, *et al.* (2015) Macrolides rapidly inhibit red blood cell invasion by the human malaria parasite, Plasmodium falciparum. *BMC Biol.* 13:52. http://dx.doi.org/10.1186/s12915-015-0162-0.
9. Waller RF, Reed MB, Cowman AF, & McFadden GI (2000) Protein trafficking to the plastid of *Plasmodium falciparum* is via the secretory pathway. *EMBO J.* 19(8):1794-1802. http://dx.doi.org/10.1093/emboj/19.8.1794.
10. Swift RP, *et al.* (2020) A mevalonate bypass system facilitates elucidation of plastid biology in malaria parasites. *PLoS Pathog.* 16(2):e1008316. http://dx.doi.org/10.1371/journal.ppat.1008316.
11. Albert A & Rees CW (1956) Avidity of the tetracyclines for the cations of metals. *Nature* 177(4505):433-434. http://dx.doi.org/10.1038/177433a0.
12. Nelson ML (1998) Chemical and biological dynamics of tetracyclines. *Adv. Dent. Res.* 12(2):5-11. http://dx.doi.org/10.1177/08959374980120011901.
13. Orth P, Schnappinger D, Hillen W, Saenger W, & Hinrichs W (2000) Structural basis of gene regulation by the tetracycline inducible Tet repressor-operator system. *Nat. Struct. Biol.* 7(3):215-219. http://dx.doi.org/10.1038/73324.
14. Marvin RG, *et al.* (2012) Fluxes in "free" and total zinc are essential for progression of intraerythrocytic stages of Plasmodium falciparum. *Chem. Biol.* 19(6):731-741. http://dx.doi.org/10.1016/j.chembiol.2012.04.013.
15. Scholl PF, Tripathi AK, & Sullivan DJ (2005) Bioavailable iron and heme metabolism in *Plasmodium falciparum*. *Curr. Top. Microbiol. Immunol.* 295:293-324.
16. Mabeza GF, Loyevsky M, Gordeuk VR, & Weiss G (1999) Iron chelation therapy for malaria: a review. *Pharmacol. Ther.* 81(1):53-75. http://dx.doi.org/10.1016/s0163-7258(98)00037-0.
17. Gisselberg JE, Dellibovi-Ragheb TA, Matthews KA, Bosch G, & Prigge ST (2013) The suf iron-sulfur cluster synthesis pathway is required for apicoplast maintenance in malaria parasites. *PLoS Path.* 9(9):e1003655. http://dx.doi.org/10.1371/journal.ppat.1003655.
18. Breuer W, Shvartsman M, & Cabantchik ZI (2008) Intracellular labile iron. *Int. J. Biochem. Cell Biol.* 40(3):350-354. http://dx.doi.org/10.1016/j.biocel.2007.03.010.
19. Grobler JA, *et al.* (2002) Diketo acid inhibitor mechanism and HIV-1 integrase: implications for metal binding in the active site of phosphotransferase enzymes. *Proc. Natl. Acad. Sci. U.S.A.* 99(10):6661-6666. http://dx.doi.org/10.1073/pnas.092056199.
20. Hare S, Gupta SS, Valkov E, Engelman A, & Cherepanov P (2010) Retroviral intasome assembly and inhibition of DNA strand transfer. *Nature* 464(7286):232-236. http://dx.doi.org/10.1038/nature08784.

370 21. Ramya TN, Mishra S, Karmodiya K, Surolia N, & Surolia A (2007) Inhibitors of
371 nonhousekeeping functions of the apicoplast defy delayed death in Plasmodium falciparum.
372 *Antimicrob. Agents Chemother.* 51(1):307-316. http://dx.doi.org/10.1128/AAC.00808-06.
373 22. Kennedy K, Crisafulli EM, & Ralph SA (2019) Delayed Death by Plastid Inhibition in
374 Apicomplexan Parasites. *Trends Parasitol* 35(10):747-759.
375 http://dx.doi.org/10.1016/j.pt.2019.07.010.
376 23. Boucher MJ & Yeh E (2019) Disruption of Apicoplast Biogenesis by Chemical Stabilization
377 of an Imported Protein Evades the Delayed-Death Phenotype in Malaria Parasites. *mSphere*
378 4(1). http://dx.doi.org/10.1128/mSphere.00710-18.
379 24. Amberg-Johnson K*, et al.* (2017) Small molecule inhibition of apicomplexan FtsH1 disrupts
380 plastid biogenesis in human pathogens. *eLife* 6. http://dx.doi.org/10.7554/eLife.29865.
381 25. Uddin T, McFadden GI, & Goodman CD (2018) Validation of Putative Apicoplast-
382 Targeting Drugs Using a Chemical Supplementation Assay in Cultured Human Malaria
383 Parasites. *Antimicrob. Agents Chemother.* 62(1). http://dx.doi.org/10.1128/AAC.01161-17.
384 26. Marlin GE & Cheng S (1979) Pharmacokinetics and tolerability of a single oral 600-mg
385 dose of doxycycline. *Med. J. Aust.* 1(12):575-576. http://dx.doi.org/10.5694/j.1326-
386 5377.1979.tb142053.x.
387 27. Adadevoh BK, Ogunnaike IA, & Bolodeoku JO (1976) Serum levels of doxycycline in
388 normal subjects after a single oral dose. *Br. Med. J.* 1(6014):880.
389 http://dx.doi.org/10.1136/bmj.1.6014.880.
390 28. Gaillard T, Boxberger M, Madamet M, & Pradines B (2018) Has doxycycline, in
391 combination with anti-malarial drugs, a role to play in intermittent preventive treatment of
392 Plasmodium falciparum malaria infection in pregnant women in Africa? *Malar. J.*
393 17(1):469. http://dx.doi.org/10.1186/s12936-018-2621-x.
394 29. Todd SR*, et al.* (2015) No visible dental staining in children treated with doxycycline for
395 suspected Rocky Mountain Spotted Fever. *J Pediatr* 166(5):1246-1251.
396 http://dx.doi.org/10.1016/j.jpeds.2015.02.015.
397 30. Draper MP*, et al.* (2013) In vitro and in vivo antimalarial efficacies of optimized
398 tetracyclines. *Antimicrob. Agents Chemother.* 57(7):3131-3136.
399 http://dx.doi.org/10.1128/AAC.00451-13.
400 31. Sigala PA, Crowley JR, Henderson JP, & Goldberg DE (2015) Deconvoluting heme
401 biosynthesis to target blood-stage malaria parasites. *eLife* 4.
402 http://dx.doi.org/10.7554/eLife.09143.

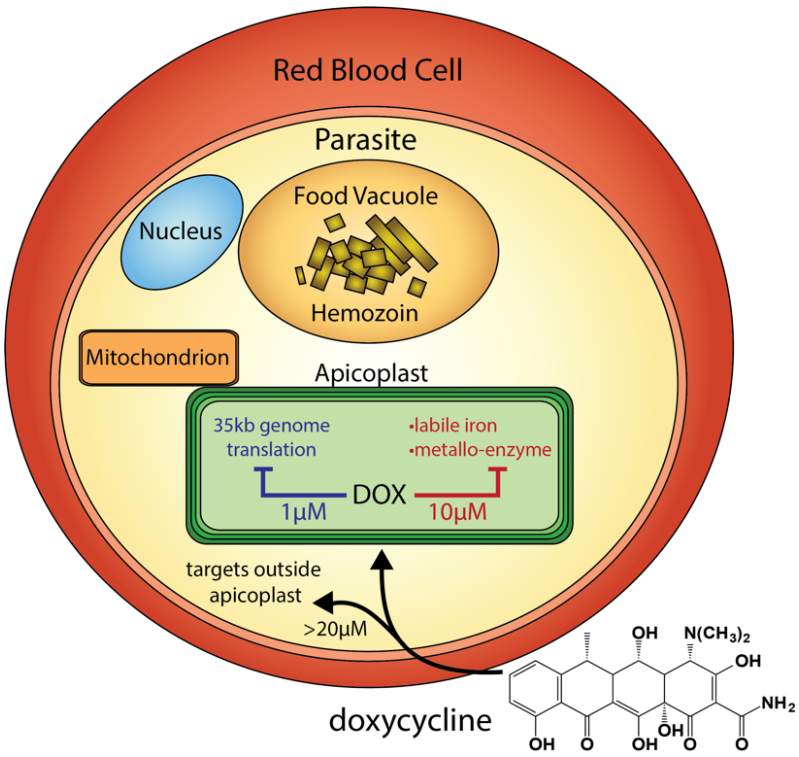

Figure 1. Scheme of intraerythrocytic *P. falciparum* parasite depicting doxycycline, its canonical delayed-death mechanism at 1 μM inhibiting apicoplast genome translation, the novel metal-dependent mechanism(s) in the apicoplast explored herein at 10 μM, and off-target activity outside the apicoplast at >20 μM.

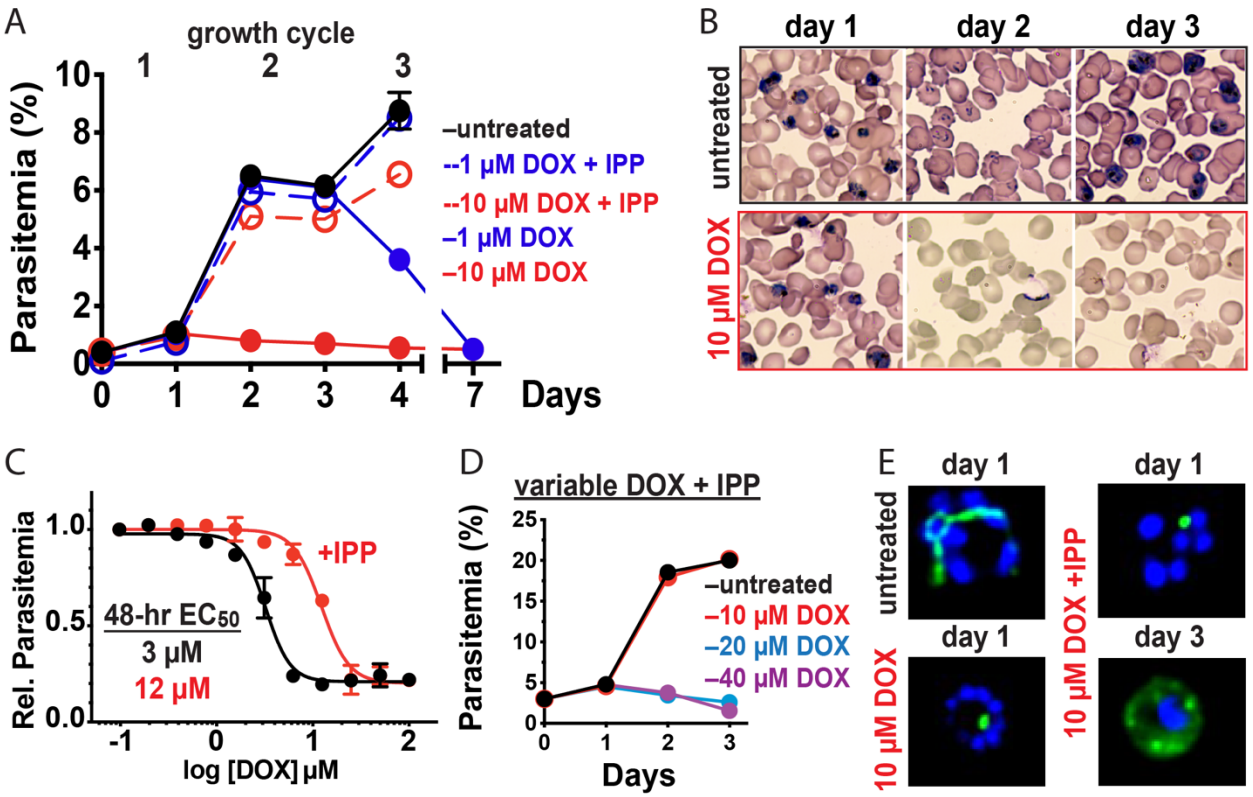

Figure 2. 10 μM doxycycline kills *P. falciparum* with first-cycle, apicoplast-specific activity. (A) Continuous growth assay of synchronized Dd2 parasites treated with 1 or 10 μM DOX ±200 μM IPP with (B) Giemsa-stained blood smears for days 1-3. (C) 48-hour growth-inhibition curve for DOX-treated Dd2 parasites ±200 μM IPP. (D) Continuous growth assay of synchronized Dd2 parasites treated with 10 – 40 μM DOX and 200 μM IPP. (E) Epifluorescence images of synchronized parasites treated as rings with 10 μM DOX ±200 μM IPP and imaged 36 or 65 hours later (green = ACP_L-GFP, blue = nuclear Hoechst stain). Data points in growth assays are the average ±SD of biological replicates. All growth assays were independently repeated 2 – 4 times using different batches of blood (shown in Figure 2- figure supplement 1).

The following figure supplements are available for figure 2:

Figure supplement 1. Additional, independent growth assays with DOX and IPP.

Figure supplement 2. Additional epifluorescence images of DOX-treated parasites and analysis.

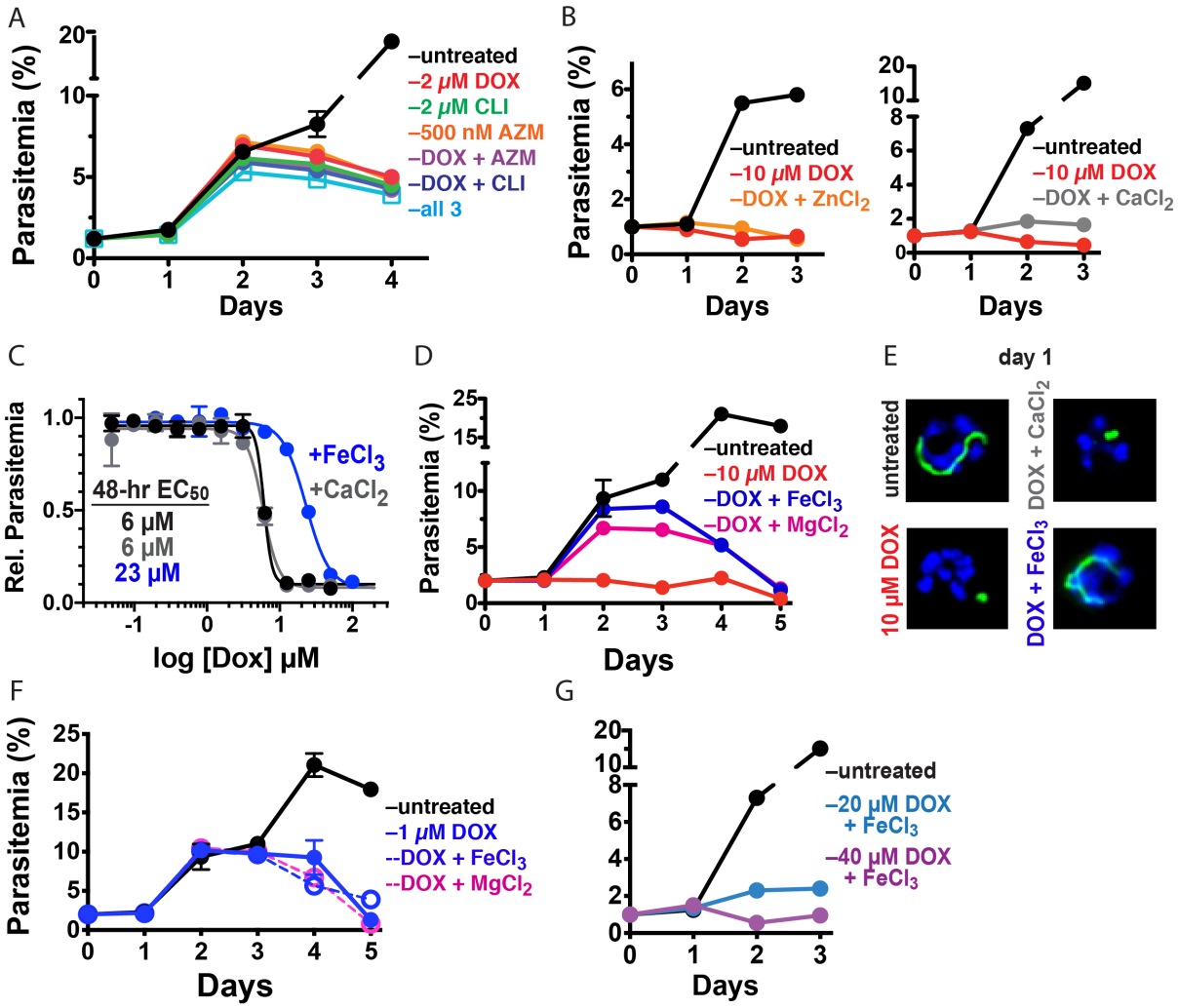

Figure 3. 10 μM DOX kills *P. falciparum* with a first-cycle, metal-dependent mechanism. Continuous growth assays of synchronized Dd2 parasites treated with (A) DOX, clindamycin (CLI), and/or azithromycin (AZM) and (B) 10 μM DOX and 10 μM $ZnCl_2$ or 500 μM $CaCl_2$. (C) 48-hour growth inhibition assay of D10 parasites treated with DOX without or with 500 μM $FeCl_3$ or $CaCl_2$. (D) Continuous growth assay of synchronized Dd2 parasites treated with 10 μM DOX and 500 μM $FeCl_3$ or $MgCl_2$. (E) Epifluorescence images of synchronized parasites treated as rings with 10 μM DOX ±500 μM $FeCl_3$ or $CaCl_2$ and imaged 36 hours later (green = ACP_L-GFP, blue = nuclear Hoechst stain). (F) Continuous growth assay of synchronized Dd2 parasites treated with 1 μM DOX and 500 μM $FeCl_3$ or $MgCl_2$. (G) Continuous-growth assay of synchronized Dd2 parasites treated with 20 or 40 μM DOX and 500 μM $FeCl_3$. Data points in growth assays are the average ±SD of biological replicates. All growth assays were independently repeated using different batches of blood (shown in Figure 3- figure supplement 1).

The following figure supplements are available for figure 3:

Figure supplement 1. Additional independent growth assays with DOX, antibiotics, and metals.

Figure supplement 2. Additional images and analysis of parasites treated with DOX and metals.

Figure supplement 3. Effect of deferoxamine on parasite growth and apicoplast biogenesis.

451 **Supplemental Figures**

452

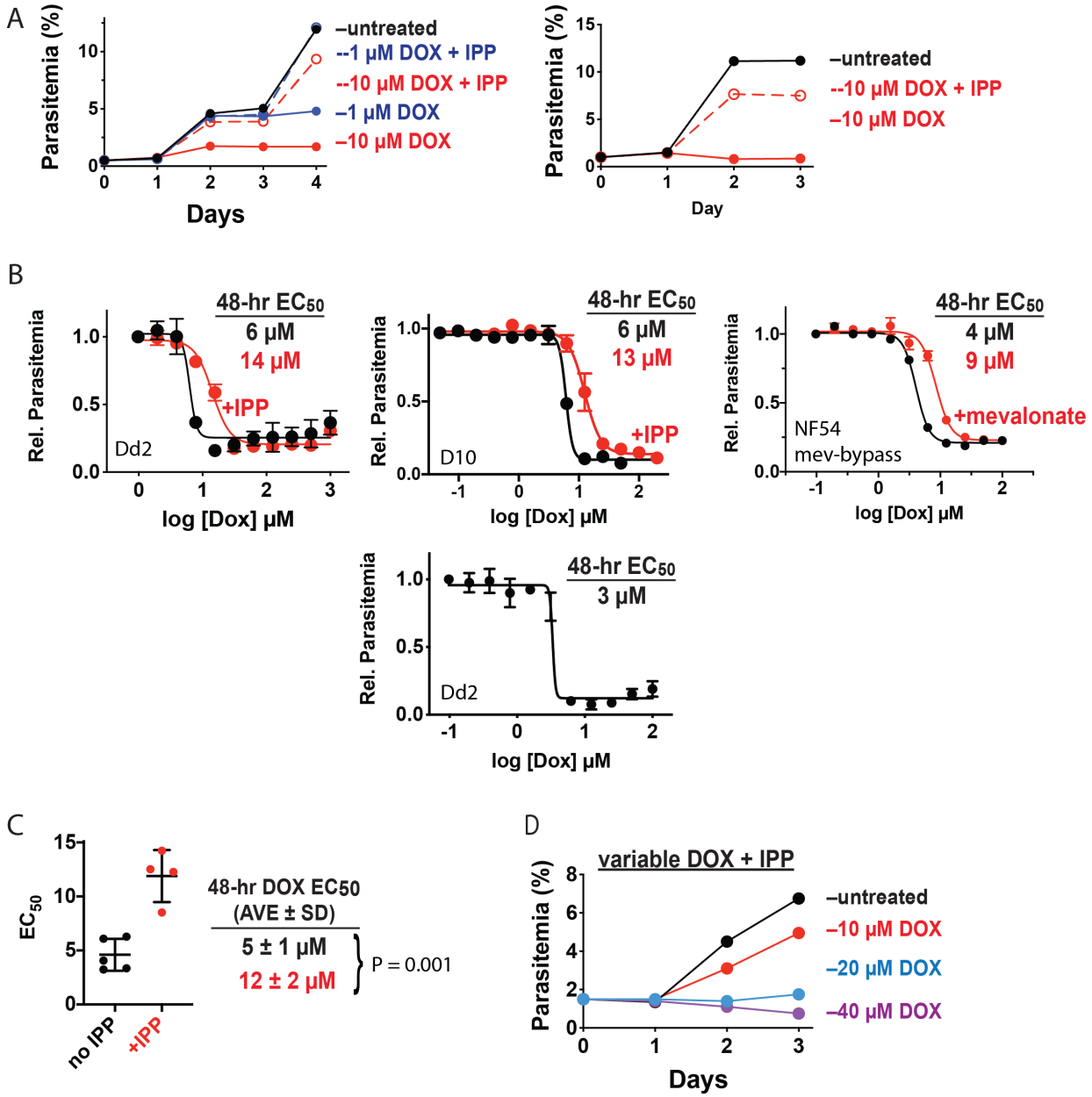

453

454 **Figure 2- figure supplement 1.** Additional, independent growth assays with DOX and IPP. (A)
455 Additional continuous growth assays of synchronized Dd2 parasites treated with 1 or 10 µM DOX
456 ±200 µM IPP. (B) Independent 48-hour growth-inhibition assays for DOX-treated Dd2, D10,
457 NF54 parasites in the absence or presence of 200 µM IPP or 50 µM mevalonate. Dd2 and NF54
458 parasites were synchronized by single treatment with 5% D-sorbitol. D10 parasites were
459 synchronized by magnet purification of schizonts followed by 5-hour incubation with uninfected
460 erythrocytes and treatment with 5% D-sorbitol. Data points in individual plots are the ave ±sd of
461 2-4 biological replicates. Each plot reflects an independent assay performed with a different batch
462 of blood. (C) Scatter plot of doxycycline EC_{50} values from independent assays ±IPP with
463 calculated ave ± sd and analysis by unpaired t-test. (D) Independent continuous growth assay of
464 synchronized Dd2 parasites treated with 10 – 40 µM DOX and 200 µM IPP.

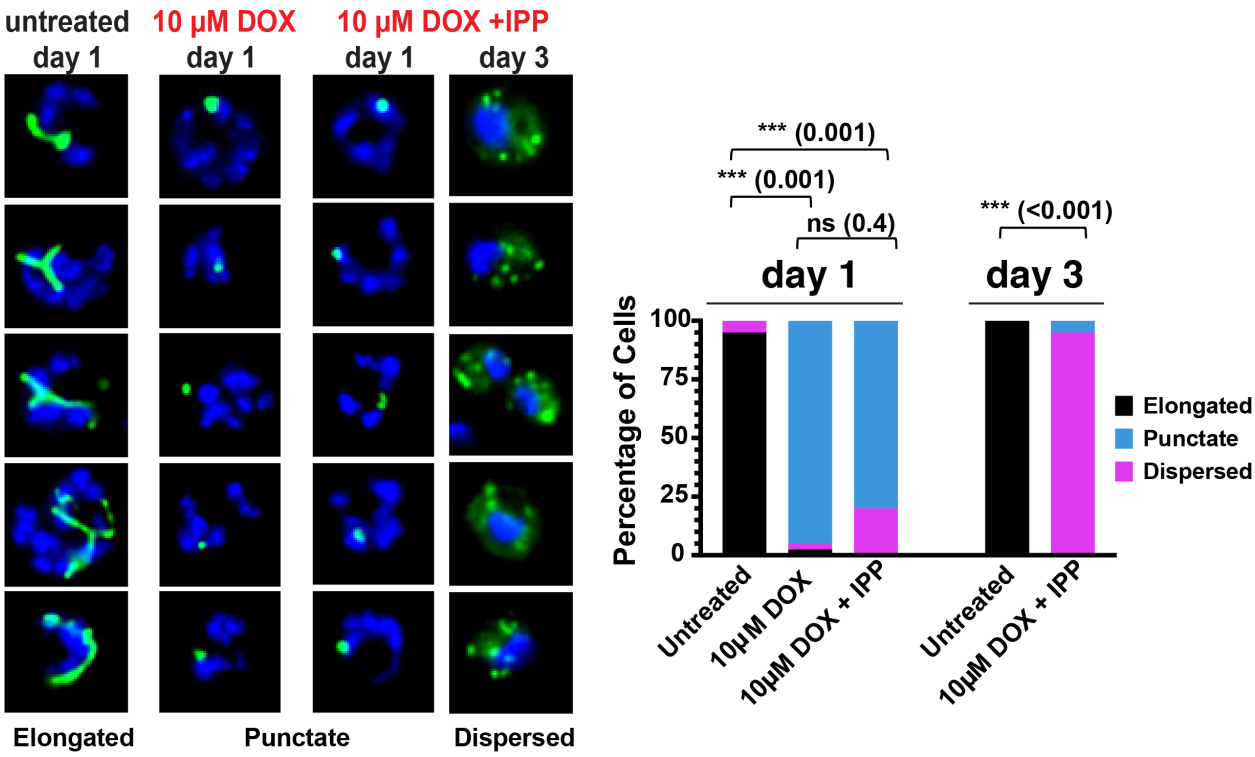

Figure 2- figure supplement 2. Additional epifluorescence images of DOX-treated D10 parasites. Magnet plus sorbitol-synchronized parasites were treated as rings with 10 µM DOX ±200 µM IPP and imaged 1 or 3 days later (green = ACP_L-GFP, blue = nuclear Hoechst stain). 20-40 parasites were examined for each treatment condition on each given day for duplicate experiments, and data were plotted as the average percentage of parasites in each population that displayed an elongated, punctate, or dispersed apicoplast GFP signal. For clarity, error bars are not displayed but standard deviations were <10% in all conditions. Cell-percentage differences were analyzed by unpaired t-test (P values in parentheses, ns = not significant).

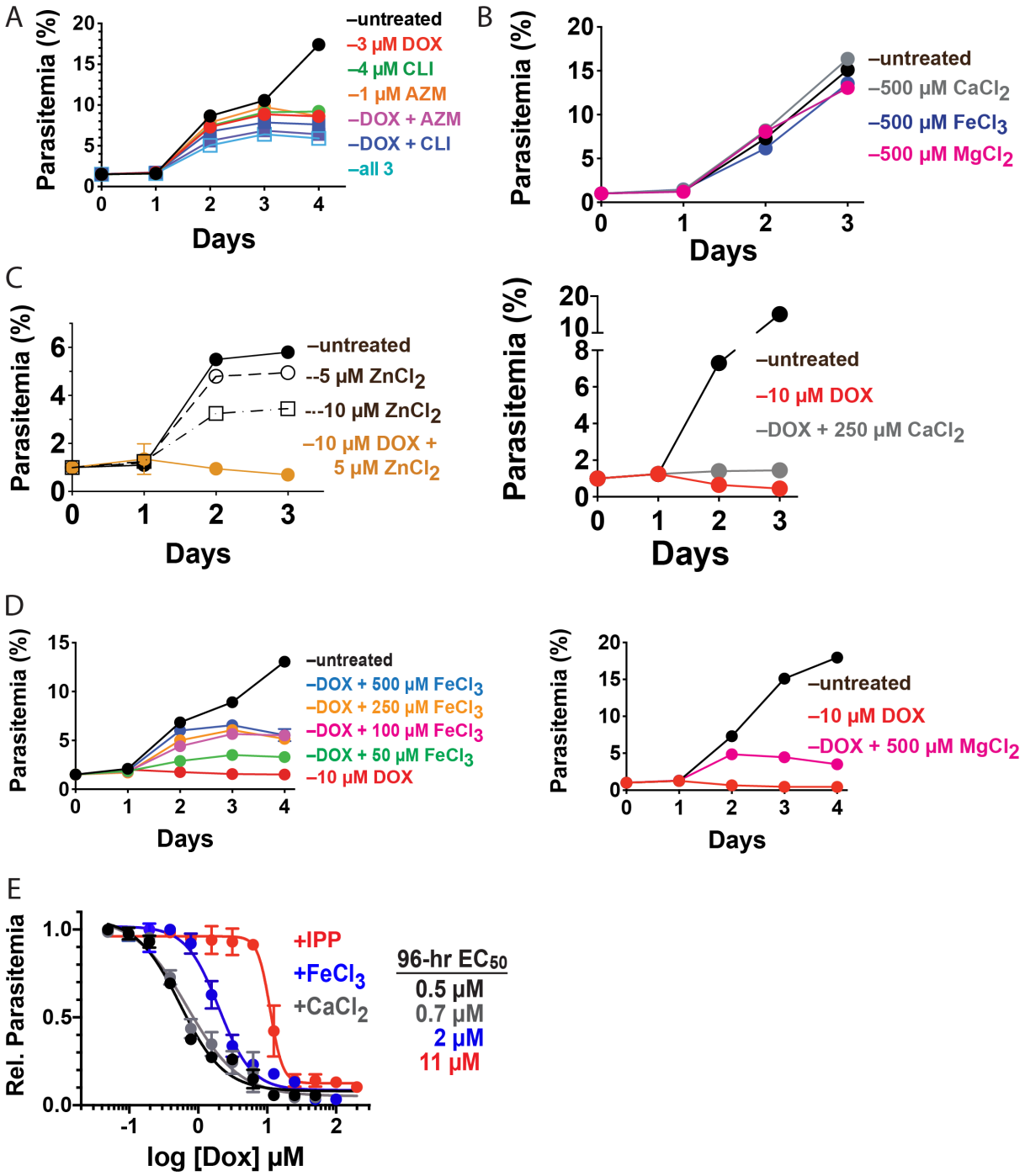

Figure 3- figure supplement 1. Additional, independent growth assays with DOX, other antibiotics, and metals. Additional continuous growth assays of synchronized Dd2 parasites treated with (A) DOX, clindamycin (CLI), and/or azithromycin (AZM); (B) 500 μM of $CaCl_2$, $MgCl_2$, or $FeCl_3$ alone; (C) 10 μM DOX and 5 μM $ZnCl_2$ or 250 μM $CaCl_2$; (D) 10 μM DOX treated with 50 - 500 μM $FeCl_3$ or 500 μM $MgCl_2$. Individual data points are the ave ± sd from 2-4 biological replicates. (E) 96-hour growth-inhibition assays for DOX-treated D10 parasites in the absence or presence of 200 μM IPP, 500 μM $FeCl_3$, or 500 μM $CaCl_2$. Parasites were synchronized by magnet purification of schizonts followed by 5-hour incubation with uninfected erythrocytes and treatment with 5% D-sorbitol. Data points are the ave ±sd of 3 biological replicates.

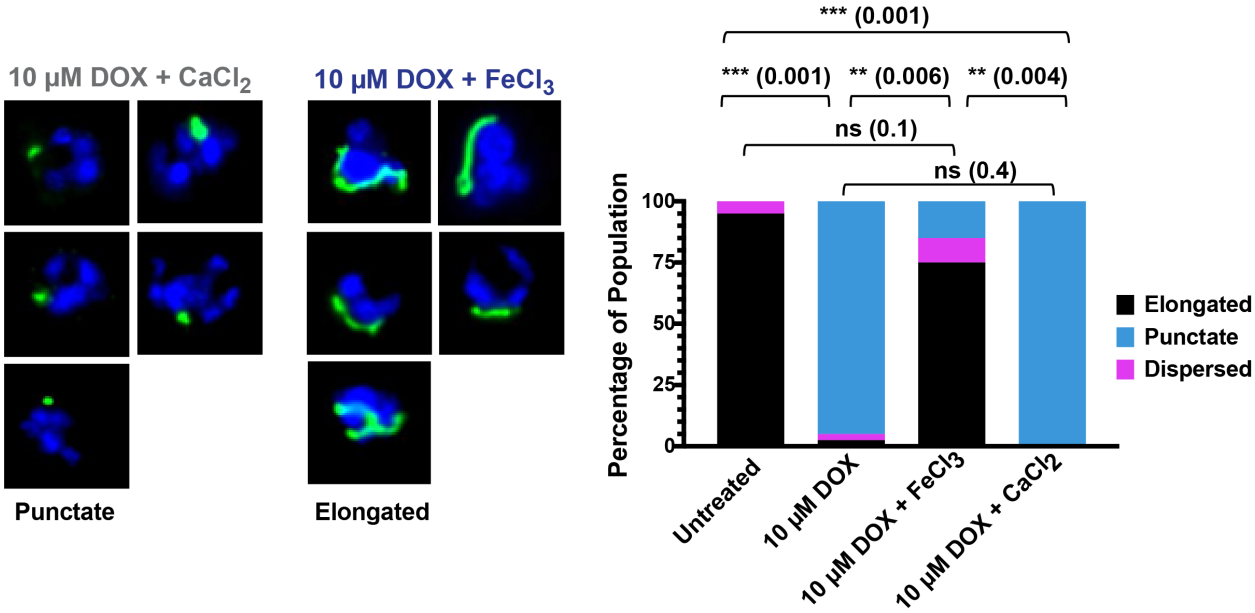

Figure 3- figure supplement 2. Additional epifluorescence images of D10 parasites treated with DOX and metals. Magnet plus sorbitol-synchronized parasites were treated as rings with 10 µM DOX ±500 µM $FeCl_3$ or $CaCl_2$ and imaged 36 hours later (green = ACP_L-GFP, blue = nuclear Hoechst stain). 20-40 parasites were examined for each treatment condition on each given day for duplicate experiments, and data were plotted as the average percentage of parasites in each population that displayed an elongated, punctate, or dispersed apicoplast GFP signal. For clarity, error bars are not displayed but standard deviations were <10% in all conditions. Cell-percentage differences were analyzed by unpaired t-test (P values in parentheses, ns = not significant).

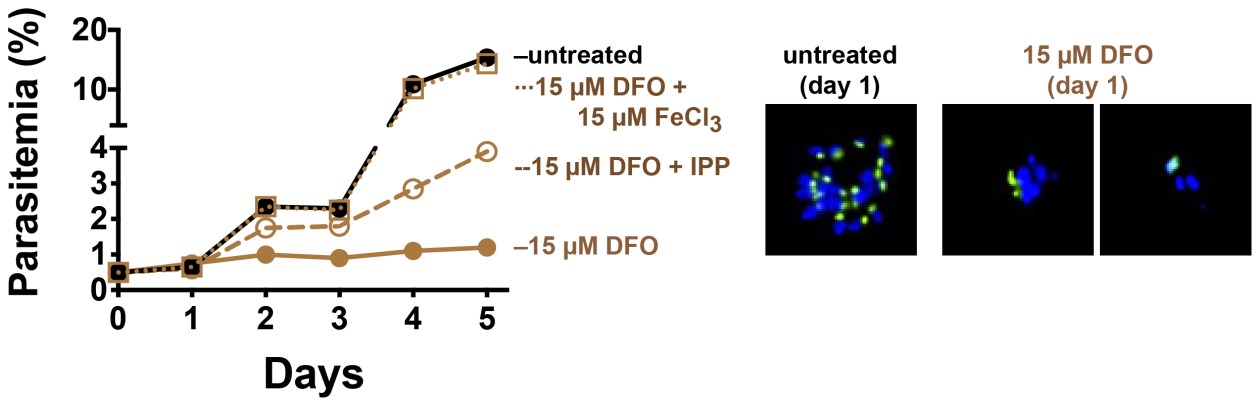

527
528 **Figure 3- figure supplement 3.** Effect of deferoxamine on parasite growth and apicoplast
529 biogenesis. (Left) Continuous growth assay of synchronized Dd2 parasites cultured without or
530 with 15 μM deferoxamine (DFO), 15 μM $FeCl_3$, or 200 μM IPP. (Right) Fluorescence microscopy
531 of live, synchronized D10 parasites untreated or treated with 15 μM DFO and imaged 36 hours
532 later (green = ACP_L-GFP, blue = nuclear Hoechst stain).